*Journal of Dynamics, Monitoring and Diagnostics*, 2022, 1, 111-124
https://doi.org/10.37965/jdmd.2022.65

ISTP
RESEARCH ARTICLE

# IGIgram: An Improved Gini Index-Based Envelope Analysis for Rolling Bearing Fault Diagnosis

**Bingyan Chen,[1] Dongli Song,[1] Yao Cheng,[1] Weihua Zhang,[1] Baoshan Huang,[2] and Yousif Muhamedsalih[3]**

[1]State Key Laboratory of Traction Power, Southwest Jiaotong University, Chengdu 610031, China
[2]School of Industrial Automation, Beijing Institute of Technology, Zhuhai 519088, China
[3]Institute of Railway Research, University of Huddersfield, Huddersfield, HD1 3DH, UK

(Received 5 December 2021; Revised 26 April 2022; Accepted 9 June 2022; Published online 10 June 2022)

***Abstract:*** The transient impulse features caused by rolling bearing faults are often present in the resonance frequency band which is closely related to the dynamic characteristics of the machine structure. Informative frequency band identification is a crucial prerequisite for envelope analysis and thereby accurate fault diagnosis of rolling bearings. In this paper, based on the ratio of quasi-arithmetic means and Gini index, improved Gini indices (IGIs) are proposed to quantify the transient impulse features of a signal, and their effectiveness and advantages in sparse quantification are confirmed by simulation analysis and comparisons with traditional sparsity measures. Furthermore, an IGI-based envelope analysis method named IGIgram is developed for fault diagnosis of rolling bearings. In the new method, an IGI-based indicator is constructed to evaluate the impulsiveness and cyclostationarity of the narrow-band filtered signal simultaneously, and then a frequency band with abundant fault information is adaptively determined for extracting bearing fault features. The performance of the IGIgram method is verified on the simulation signal and railway bearing experimental signals and compared with typical sparsity measures-based envelope analysis methods and log-cycligram. The results demonstrate that the proposed IGIs are efficient in quantifying bearing fault-induced transient features and the IGIgram method with appropriate power exponent can effectively achieve the diagnostics of different axle-box bearing faults.

***Key words:*** envelope analysis; fault diagnosis; frequency band identification; improved Gini indices; railway bearings

## I. INTRODUCTION

Rolling bearings are widely used in rotating machinery equipment in the fields of transportation, energy and chemical industries, such as high-speed trains, aero engines, automobile engines, wind turbine generator sets, and steam turbine generator sets. Unexpected damage or failure in rolling bearings may lead to serious human injury or huge economic losses [1]. Thus, fault diagnosis of rolling bearings in key transportation, energy and chemical equipment is of great significance to ensure operational safety and improve economic benefits. Up to now, many signal processing-based methods have been developed for fault diagnosis of rolling bearings, such as blind deconvolution [2], signal decomposition [3], envelope analysis [4], stochastic resonance [5,6], morphological filtering [7], cyclic spectral analysis [8,9] and modulation signal bispectrum [10]. Among these methods, envelope analysis is one of the most commonly used methods for fault diagnosis of rolling bearings and other rotating mechanical components. In this method, band-pass filtering is usually performed on a resonance frequency band to extract the fault-caused transient impulses hidden in the noisy vibration signals [11]. Therefore, informative frequency band identification (IFBI) is a crucial prerequisite for rolling bearing fault diagnosis based on envelope analysis.

At present, many IFBI methods have been established for fault diagnosis of rolling bearings, which can be roughly divided into blind methods and targeted methods [12]. It should be emphasized that the "blind" and "targeted" here are only for the characteristics of the frequency band identification criteria rather than the method itself and its implementation process. This is a key point to note so as not to cause ambiguity.

The blind IFBI method makes no assumptions about the periodicity of the bearing fault features in the analyzed signal [12], and can adaptively identify an informative frequency band (IFB) closely related to transient fault features. A representative blind IFBI method is the fast kurtogram proposed by Antoni [4]. In this method, a 1/3-binary tree filter bank is designed to split the vibration signal into a group of narrowband filtered signals with different center frequencies and bandwidths, and the kurtosis of the narrowband filtered signal is taken as a criterion to identify the IFB by evaluating the impulsiveness of bearing fault features. However, the fast kurtogram tends to select the fault-unrelated frequency band when confronted with vibration signals polluted by strong random impulse noise, which may attribute to the inherent limitation of kurtosis susceptible to outliers. Subsequently, the protrugram [13] was developed for IFBI by employing the kurtosis of the envelope spectrum of the narrowband filtered signal as the evaluation criterion of the fault information. The autogram was proposed for bearing diagnosis in [14] by using the kurtosis of the autocorrelation of the squared envelope of the filtered signal as the frequency band identification criterion. Similarly, correlation spectral negentropy was proposed in [15] to identify IFB. Since the protrugram is dedicated to evaluating the cyclostationarity

Corresponding author: Dongli Song, (e-mail: sdl.cds@163.com)

 

rather than the impulsiveness of bearing fault features and the autogram aims to characterize the periodicity of bearing fault features, they are more robust to random impulse noise in comparison with the fast kurtogram. However, the protrugram delivers low robustness to discrete harmonic interference from shaft rotation or gear meshing, which exhibits a high-level peak in the envelope spectrum; the autogram has difficulty extracting the desired repetitive transient fault features when strong discrete harmonics are present. Tse and Wang [16] used the ratio of L2 to L1 norm (L2/L1) of the power spectrum of the narrowband filtered signal to determine IFB for bearing fault diagnosis. However, L2/L1 is also susceptible to large outliers, thus its normalized version namely Hoyer index (HI) [17] may be an alternative evaluation criterion. Antoni [18] fused both the impulsiveness and cyclostationarity into the infogram using the arithmetic mean of the negentropy (NE) of the squared envelope and the NE of the squared envelope spectrum (SES) for IFBI. Hebda-Sobkowicz et al. [19] replaced the arithmetic mean of partial infograms with the logarithmic mean, geometric mean and normalizing of partial infograms to improve the robustness of the classical infogram to non-Gaussian noise. HI and NE have weaker sensitivity to random impulses compared with kurtosis, but they also show poor IFBI performance in the presence of strong random impulses. In addition, Gini index (GI), originally used in the field of economics, was introduced into the field of mechanical fault diagnosis to quantify impulse features and guide the selection of IFB [20,21]. GI is less sensitive to non-Gaussian noise than kurtosis, NE and HI, whereas its fault-impulse discernibility is weaker than kurtosis, NE and HI [22]. Thus, it is necessary to develop robust transient feature quantification metrics for improving the accuracy of frequency band identification. In addition, the L-kurtosis [23], stability index [24], conditional variance statistic [25], averaged local kurtosis [26] and subband averaging kurtogram [27] were proposed to distinguish bearing fault-related frequency band in the presence of non-Gaussian noise. The works in [21,22,28,29] summarized and compared the performance of typical blind IFBI methods in bearing fault diagnosis.

The targeted IFBI method focuses on the (quasi) periodicity of bearing fault features to extract the cyclic components in the signal to be analyzed, requiring knowledge of the impulse period (in the time domain) or the fault characteristic frequency (in the frequency domain) before identifying IFB. For example, the harmonic-to-noise ratio [30] and correlated kurtosis [31,32] using the impulse period have been employed to construct the IFBI methods for extracting periodic bearing fault features. In recent years, the cyclostationarity of bearing fault signals has received increasing attention, and the IFBI methods using fault characteristic frequency have been continuously proposed, such as the ratio of cyclic content [33], indicator of second-order cyclostationarity [34], frequency domain correlated kurtosis [35] and weighted cyclic harmonic-to-noise ratio [36]. These methods mainly use the SES and the fault characteristic frequency of interest to construct the evaluation indicator of cyclostationarity as the frequency band identification criterion. Inspired by the works in [37,38] where the log-envelope spectrum was discovered to be a robust tool for characterizing cyclostationarity in the presence of high impulse noise, the IFBI methods based on the log-envelope spectrum were established, such as log-cycligram (LC) [12], cyclic harmonic ratio [39] and LEASgram [40]. In addition, by exploiting the insensitivity of correntropy to impulse noise, FECgram [41] was proposed to identify IFB for bearing diagnostics. The works in [12,42] comparatively investigated the performance of the blind and targeted IFBI methods in distinguishing IFB. Benefiting from the frequency band identification criteria using impulse period or fault characteristic frequency, the targeted IFBI methods are generally more robust than the blind IFBI methods in the presence of high impulsive noise. However, the targeted IFBI methods require an accurate impulse period or fault characteristic frequency as a prerequisite to ensure the accurate identification of fault-related frequency bands. In contrast, the blind IFBI methods do not require impulse period and fault characteristic frequency in distinguishing fault-related frequency band, thus exhibiting wider adaptability. Therefore, this paper aims to develop a blind IFBI method which is robust to impulse noise and can achieve fault diagnosis performance similar to those of the targeted IFBI methods.

In recent years, the design of new quantitative indicators of machine fault features has received increasing attention. Wang et al. [43] proposed the sum of weighted normalized squared envelope as a framework to characterize the repetitive transients for machine condition monitoring. Hou et al. [44] discovered that typical sparsity measures can be reformulated into the ratio of different quasi-arithmetic means (RQAM). RQAM has been proved to be a powerful tool for designing quantitative indicators for characterizing repetitive transients [44–46]. To improve the accuracy of IFBI for bearing fault diagnosis, the design of new sparsity measures and their application in bearing fault diagnosis are investigated. The main novelties and contributions of this paper include:

(1) Based on RQAM, a novel generalization method of GI is developed, which allows the single parameter generalization of classic GI by using the power function-based quasi-arithmetic means and leads to new quantitative indicators named improved GIs (IGIs) for quantifying transient features.

(2) The sparse quantization capability and repetitive transient discriminability of IGIs are investigated using simulations, and the results show that IGIs exhibit rich sparse quantization capabilities and can achieve improved repetitive transient discriminability compared with traditional sparsity measures.

(3) An IGI-based IFBI method named IGIgram is proposed for bearing fault diagnosis, which utilizes IGI to adaptively identify an IFB with rich fault information by evaluating both the impulsiveness and cyclostationarity of bearing fault features.

(4) The effectiveness of IGIgram is validated using simulation and experimental signals, and the results confirm that IGIgram with appropriate power exponent can achieve accurate IFBI for effective extraction of repetitive transients and fault diagnosis of railway axle-box bearings.

The remainder of this paper is arranged as follows. In Section II, the traditional sparsity measures for IFBI are briefly reviewed and the formal definition and performance analysis of IGIs are presented. Section III introduces the envelope analysis method based on IGIs for bearing fault diagnosis. In Sections IV and V, the simulation signals and railway axle-box bearing experimental signals are analyzed to validate the effectiveness of the proposed fault diagnosis

method, and the performance is compared with the IFBI methods based on typical sparsity measures. Section VI presents the comparison results with the LC method. The main conclusions of this paper are summarized in Section VII.

# II. TRADITIONAL AND NOVEL SPARSITY MEASURES

## A. TRADITIONAL SPARSITY MEASURES

Sparsity measures are usually regarded as the measure of the energy concentration of a signal [47]. Specifically, if all energy is concentrated in one element of the signal, the sparsity value of the signal is maximum. On the contrary, if all elements have the same energy, the sparsity of the signal is minimum. Let $\boldsymbol{x} = [x_1, x_2, \cdots, x_N]$ be a discrete vibration signal with $N$ samples, the typical sparsity measures for characterizing transient impulse features in IFBI are introduced as follows.

Kurtosis (Kurt) [48]:

$$\text{Kurt} = \frac{1}{N}\sum_{n=1}^{N} x_n^4 \Big/ \left(\frac{1}{N}\sum_{n=1}^{N} x_n^2\right)^2 \tag{1}$$

Negentropy [18]:

$$\text{NE} = \frac{1}{N}\sum_{n=1}^{N} \frac{x_n^2}{\frac{1}{N}\sum_{n=1}^{N} x_n^2} \ln \frac{x_n^2}{\frac{1}{N}\sum_{n=1}^{N} x_n^2} \tag{2}$$

Ratio of L2 to L1 norm (L2/L1) [16]:

$$\text{L2/L1} = \sqrt{N}\frac{\|\boldsymbol{x}\|_2}{\|\boldsymbol{x}\|_1} \tag{3}$$

Hoyer index [17]:

$$\text{HI} = \left(\sqrt{N} - \frac{\|\boldsymbol{x}\|_1}{\|\boldsymbol{x}\|_2}\right) \Big/ (\sqrt{N} - 1) \tag{4}$$

Gini index [49]:

$$\text{GI} = 1 - \sum_{n=1}^{N} \frac{x_{(n)}}{\|\boldsymbol{x}\|_1}\left(\frac{2(N-n)+1}{N}\right) \tag{5}$$

where $\|\boldsymbol{x}\|_1$ and $\|\boldsymbol{x}\|_2$ denote the L1 norm and L2 norm, respectively; $\boldsymbol{x}_{asc} = [x_{(1)}, x_{(2)}, \cdots, x_{(N)}]$ is the permutation of sequence $\boldsymbol{x} = [x_1, x_2, \cdots, x_N]$ in ascending order, i.e., $x_{(1)} \le x_{(2)} \le \cdots \le x_{(N)}$. Note that the input sequence of GI is nonnegative.

These sparsity measures are typical indicators of transient impulse features in a signal and have been applied to the condition monitoring and fault diagnosis of rolling bearings by characterizing the impulsiveness or cyclostationarity of bearing fault signals. However, traditional sparsity measures have exposed some shortcomings in practical applications. The value of kurtosis varies largely with the signal amplitude, especially outliers, which is not conducive to the detection of bearing fault impulses in industrial scenarios. Moreover, the range of kurtosis cannot be accurately estimated. The sensitivity of NE, L2/L1 and HI to outliers is lower than kurtosis, but their fault impulse detection performance will still be affected when encountering strong random impulses [22,50]. GI is robust to outliers and has a clear range of [0,1], but its ability to identify bearing fault impulses under noise interference is weaker than kurtosis and NE [22]. Therefore, it is necessary to develop new sparsity measures that are robust to random impulses and background noise for transient feature characterization and bearing fault diagnosis.

## B. IMPROVED GINI INDICES

To overcome the limitations of traditional sparsity measures in characterizing transient impulse features and detecting bearing faults, new sparsity measures or statistical indicators have been explored recently. Based on RQAM, Hou et al. [45] proposed generalized Gini indices (GGIs) by introducing the nonlinear weights into the classic GI, as follows:

$$\text{GGI} = 1 - \sum_{n=1}^{N} w_n x_{(n)} \Big/ \sum_{n=1}^{N} \frac{x_n}{N} \tag{6}$$

where $w_n = [2(N-n)+1]^a / \sum_{n=1}^{N} [2(N-n)+1]^a$ is the nonlinear weight and $a > 0$ is the weight parameter.

Compared with GI and other traditional sparsity measures, GGIs can achieve different sparse quantization capabilities and tunable random transient resistibility by adjusting weight parameter. However, the repetitive transient discriminability of GGIs with different weight parameters shows small differences and is inferior to Kurt, NE and HI, which will be elucidated in Section II.C. Moreover, both GI and GGIs employ a line function as the generator of the quasi-arithmetic means. Given the nonlinear property of power functions, it is worth investigating the construction of sparsity measures by using quasi-arithmetic means based on power function. Therefore, based on RQAM and classical GI, IGIs are proposed as a new family of statistical indicators, as follows:

$$\begin{aligned}\text{IGI} &= 1 - \sqrt[p]{\sum_{n=1}^{N} w_n' x_{(n)}^p \Big/ \sum_{n=1}^{N} \frac{x_n^p}{N}} \\ &= 1 - \sqrt[p]{\sum_{n=1}^{N} \frac{x_{(n)}^p}{\|\boldsymbol{x}\|_p^p}\left(\frac{2(N-n)+1}{N}\right)}\end{aligned} \tag{7}$$

where $\|\boldsymbol{x}\|_p$ is the Lp norm, $p > 0$ is the power exponent, $w_n' = [2(N-n)+1]/N^2$ and $\sum_{n=1}^{N} w_n' = 1$. IGIs are reduced to GI when the power exponent $p = 1$. The power exponent of IGIs allows their performance or capability to be tunable. In addition, the definition in Eq. (7) indicates the following important properties:

- IGIs are scale-invariant, which means that the amplitude of each element multiplied by a constant factor will not change IGIs of a signal.
- IGIs are positive and their values are always between 0 and 1.

A numerical example is used to illustrate the motivation for using power functions to construct quasi-arithmetic means, as shown in Fig. 1. Fig. 1a displays a non-negative sequence ($p = 1$) with the largest element greater than 1 and its square ($p = 2$) and square root ($p = 0.5$). Fig. 1b displays a non-negative sequence with the largest element less than 1 and its square ($p = 2$) and square root ($p = 0.5$). Two prominent impulses can be observed in the original sequence (i.e., power exponent $p = 1$). For sequences with power exponents $p = 1$, 2 and 0.5, the ratios of the largest element to the smallest element of the three sequences are 72.88, 5310.97 and 8.54, respectively. Note that the quantization results for the sequences shown in

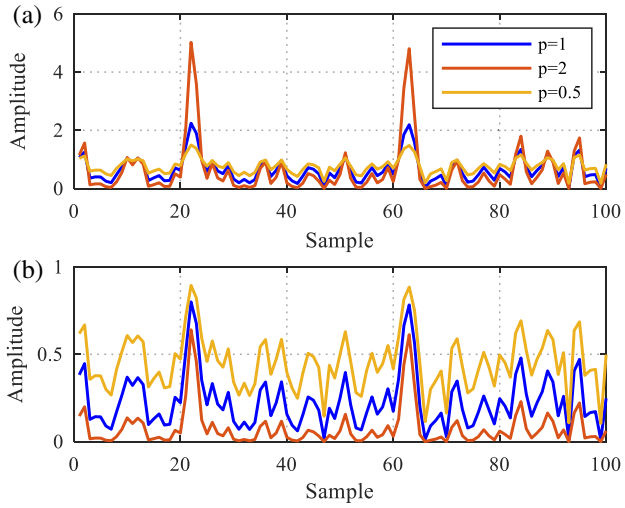


**Fig. 1.** Non-negative sequence ($p = 1$) and its square ($p = 2$) and square root ($p = 0.5$): (a) the largest element of the sequence is greater than 1, and (b) the largest element of the sequence is less than 1.

Fig. 1a, b are the same. It can be discovered that the nonlinear characteristic of the power function can be used to non-uniformly scale the sequence amplitude. Furthermore, increasing the power exponent $p$ of the sequence can increase the salience of the impulses relative to other elements, regardless of whether the largest element of the non-negative sequence is greater than 1.

As shown in Eq. (7), a linear weight sequence is applied to the normalized sequence $x^p_{(1)}/\|\boldsymbol{x}\|^p_p$, $x^p_{(2)}/\|\boldsymbol{x}\|^p_p, \ldots, x^p_{(N)}/\|\boldsymbol{x}\|^p_p$ when calculating the IGI of the sequence. Since increasing the power exponent $p$ can increase the salience of the impulses relative to other elements, it can increase the sensitivity of the IGI to transient features. Conversely, decreasing the power exponent $p$ can reduce the salience of the impulses relative to other elements, thereby increasing the resistibility of the IGI to random transients. Therefore, the power exponent of IGI allows its performance or capability to be tunable. The following numerical analysis will confirm these properties of IGI.

## C. PERFORMANCE ANALYSIS

This section illustrates the important properties of IGIs in transient feature characterization by simulation signals, and the performance is compared with existing sparsity measures, including Kurt, NE, L2/L1, HI, GI and GGIs.

Bernoulli distributions with different success probabilities are often used to generate data sequences with different sparsity [45,47]. To evaluate the sparse quantification capability of IGIs, a series of data sequences with different sparsity were generated when the success probability of the Bernoulli distribution is increased from 0.005 to 1 in increments of 0.005. The length of each data sequence is 20,000 data points. Figs. 2 and 3 show the GGIs with different weight parameters and the IGIs with different power exponents of the data sequences generated by the Bernoulli distribution with different success probabilities, respectively. The weight parameter $a$ of GGIs includes increasing from 0.1 to 1 in increments of 0.1 and from 1.5 to 10 in increments of 0.5. The power exponent $p$ of IGIs includes increasing from 0.1 to 1 in increments of 0.1 and from 1.5 to 10 in increments of 0.5. Five traditional sparsity measures are also displayed for comparison. Note that all indicators are scaled between 0 and 1.

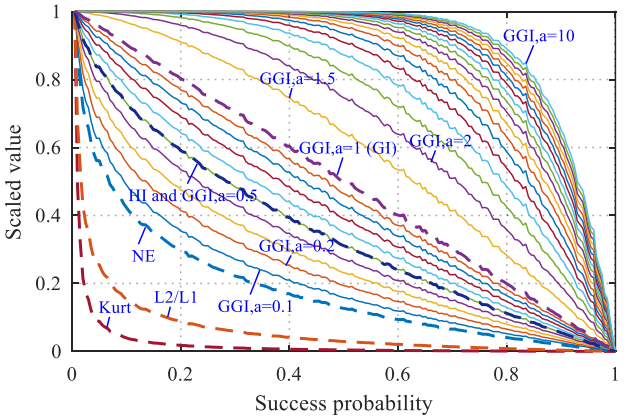


**Fig. 2.** Traditional sparsity measures and GGIs with different weight parameters of the data sequences generated by Bernoulli distribution with different success probabilities.

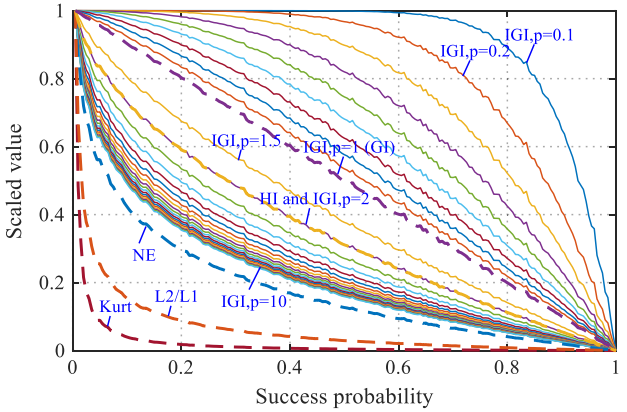


**Fig. 3.** Traditional sparsity measures and IGIs with different power exponents of the data sequences generated by Bernoulli distribution with different success probabilities.

When the success probability of the Bernoulli distribution increases from 0.005 to 1, the sparsity of the data sequence gradually becomes weaker. Similar to GGIs, IGIs with different power exponents can monotonically quantify the sparsity of a data sequence, i.e., increase gradually as the sparsity of the data sequence increases. It can be observed that the sparse quantization capability of IGIs can be tuned by changing the power exponent. In addition, the descending gradient of the sparse quantization curve can reflect the random transient resistibility of the indicator. The smaller the descending gradient, the stronger the random transient resistibility of the indicator. The results show that decreasing the power exponent can improve the random transient resistibility of IGIs, and IGIs with appropriate power exponents show stronger random transient resistibility than the five traditional sparsity measures. Therefore, IGIs and GGIs exhibit similar characteristics in random transient resistibility.

Repetitive transient features caused by defects in rotating machinery are often contaminated by background noise,

thus, the repetitive transient discriminability is of great importance for the indicators. To evaluate the repetitive transient discriminability of IGIs, a set of mixed signals of the periodic impulses $s_p(t)$ and Gaussian noise $s_n(t)$ are generated by changing the SNR of Gaussian noise. 100 impulses are evenly distributed in the periodic impulse signal. The Gaussian noise is generated by the "awgn" function in MATLAB. The periodic impulse signal and Gaussian noise signal have a length of 20,000 data points. The sampling frequency is assumed as 20,000 Hz.

$$s(t) = s_p(t) + s_n(t) \tag{8}$$

$$s_p(t) = 2\sum_{i=1}^{100} e^{-1000(t-i/100)} \sin(2\pi \cdot 3500(t - i/100)) \tag{9}$$

Figs. 4 and 5 exhibit the GGIs with different weight parameters and IGIs with different power exponents of the envelopes of the mixed signals of periodic impulses and Gaussian noise when SNR is increased from −20 dB to 40 dB in increments of 0.1 dB, respectively. Figure 6 shows the partial enlargements of Figs. 4 and 5. The weight parameter $a$ of GGIs includes increasing from 0.1 to 1 in increments of 0.1 and from 1.5 to 10 in increments of 0.5. The power exponent $p$ of IGIs includes increasing from 0.1 to 1 in increments of 0.1 and from 1.5 to 10 in increments of 0.5. Five traditional

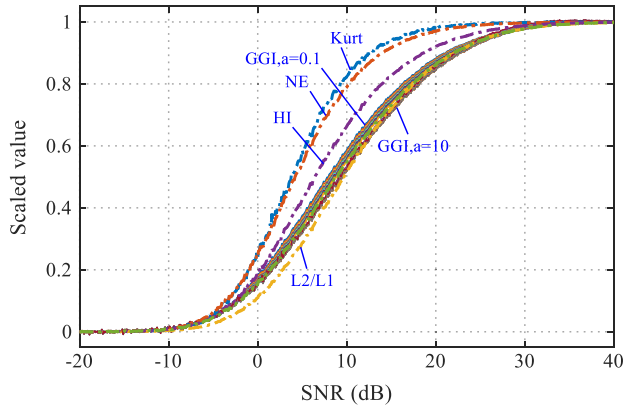


**Fig. 4.** Traditional sparsity measures and GGIs with different weight parameters of the envelopes of the mixed signals of periodic impulses and Gaussian noise with different SNRs.

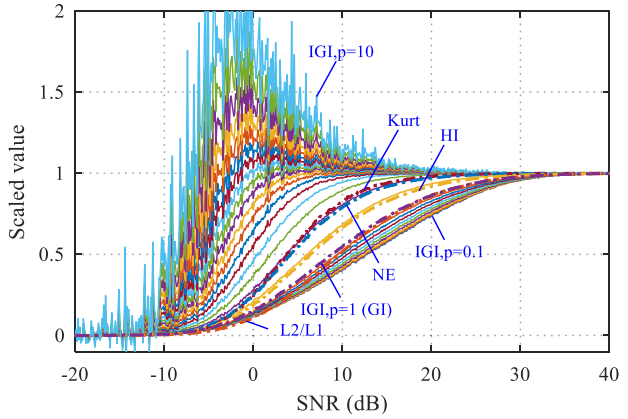


**Fig. 5.** Traditional sparsity measures and IGIs with different power exponents of the envelopes of the mixed signals of periodic impulses and Gaussian noise with different SNRs.

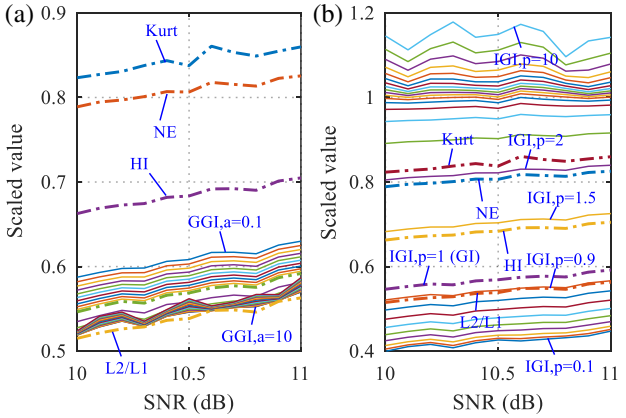


**Fig. 6.** (a) Partial enlargement of Fig. 4 and (b) partial enlargement of Fig. 5.

sparsity measures are also displayed for comparison. Note that all indicators are scaled by using Eq. (10):

$$S_{\text{scaled}}(m) = \frac{S_{\text{mixed}}(m) - S_{\text{noise}}(m)}{S_{\text{impulse}} - S_{\text{noise}}(m)} \tag{10}$$

where $S_{\text{mixed}}(m)$ and $S_{\text{noise}}(m)$ are the indicator values of the envelopes of the mixed signal and Gaussian noise signal under an SNR of $m$, respectively; $S_{\text{impulse}}$ is the indicator value of the envelopes of the periodic impulse signal; $S_{\text{scaled}}(m)$ is the scaled indicator value under an SNR of $m$.

When the SNR increases from −20 dB to 40 dB, the scaled indicator value gradually increases from 0 to 1, and the increasing gradient of the quantization curve can reflect the repeated transient identification ability of the index. The greater the increasing gradient, the stronger the repetitive transient discriminability of the indicator. Figs. 4 and 6a show that the repetitive transient discriminability of GGIs with different weight parameters is similar to that of classical GI and inferior to Kurt, NE and HI. Reducing the weight parameter can slightly improve the repetitive transient discriminability of GGIs, but the effect of the weight parameter on improving the repetitive transient discriminability of GGIs is limited. In contrast, IGIs with different power exponents exhibit rich repetitive transient discriminability and can achieve stronger repetitive transient discriminability than five traditional sparsity measures and GGIs with different weight parameters, as exhibited in Figs. 5 and 6b. In addition, increasing the power exponent can effectively improve the repetitive transient discriminability of IGIs, but too high power exponents make IGIs susceptible to interference noise.

The above results lead to the following important remarks: (1) IGIs with different power exponents can quantify the sparsity of data sequences; (2) IGIs with appropriate power exponents can simultaneously possess strong random transient resistibility and repetitive transient discriminability; (3) IGIs with appropriate power exponents can achieve excellent transient feature quantization compared to traditional sparsity measures.

## III. IMPROVED GINI INDEX-GUIDED ENVELOPE ANALYSIS

Recently, Hebda-Sobkowicz et al. [19] investigated the extension of the classic infogram by substituting the

arithmetic mean with the weighted mean, logarithmic mean and geometric mean for IFBI. The experimental results showed that the infogram based on the geometric mean (called geometric infogram) performs better than the arithmetic mean and logarithmic mean in bearing diagnostics. Inspired by the geometric infogram, the geometric mean of squared envelope IGI and squared envelope spectrum IGI (abbreviated as GMIGI) is proposed as the new criterion for IFBI, as follows:

$$\mathrm{GMIGI} = \sqrt{\mathrm{IGI_{SE}}\mathrm{IGI_{SES}}} \tag{11}$$

where $\mathrm{IGI_{SE}}$ and $\mathrm{IGI_{SES}}$ are the IGI values calculated from the squared envelope and squared envelope spectrum (SES), respectively.

In envelope analysis, frequency band division is the prerequisite for IFBI to extract fault impulse features from noisy machine vibration signals. The 1/3-binary tree filter bank [4] has the merits of high computational efficiency and variable bandwidth, thus it is adopted in this study for frequency band division. For each decomposition level $k$ of the filter bank, $k = 0,1,1.6,2,2.6,3, \cdots$, the full frequency band $[0,F_s/2]$ is split into $2^k$ narrow frequency bands with equal bandwidth $F_s/2^{k+1}$, where $F_s$ denotes the sampling frequency, as shown in Fig. 7. Further, a total of $2^k$ narrowband filtered signals can be obtained correspondingly by band-pass filtering. The details of the 1/3-binary tree filter bank are reported in [4].

On the basis of frequency band division, GMIGI is employed to evaluate the bearing fault features contained in the narrowband filtered signals. Finally, the GMIGI values of different narrow bands can form a two-dimensional map, named IGIgram, which can be used to identify an optimal narrowband filtered signal with abundant transient impulse features for fault diagnosis. A flowchart of IGI-guided envelope analysis for bearing fault diagnosis is shown in Fig. 8. The implementation procedure of the proposed fault diagnosis method is described as follows:

*Step 1:* Collect the bearing vibration signals using data acquisition equipment and acceleration sensors.

*Step 2:* Conduct band-pass filtering on the measured vibration signal by the 1/3-binary tree filter bank to generate a group of narrowband filtered signals with different bandwidths and center frequencies.

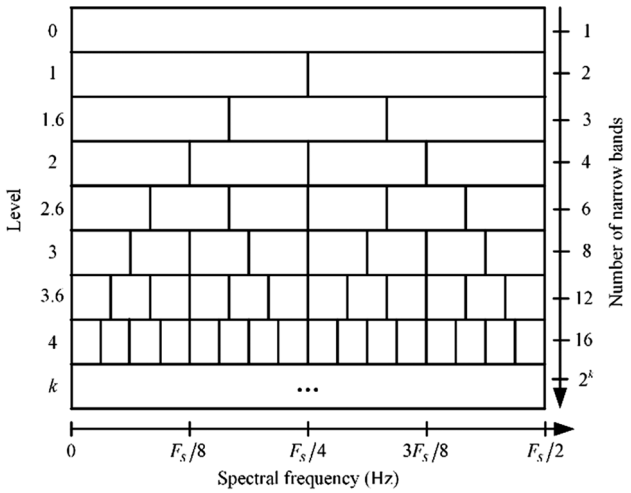


**Fig. 7.** Structure of 1/3-binary tree frequency bands.

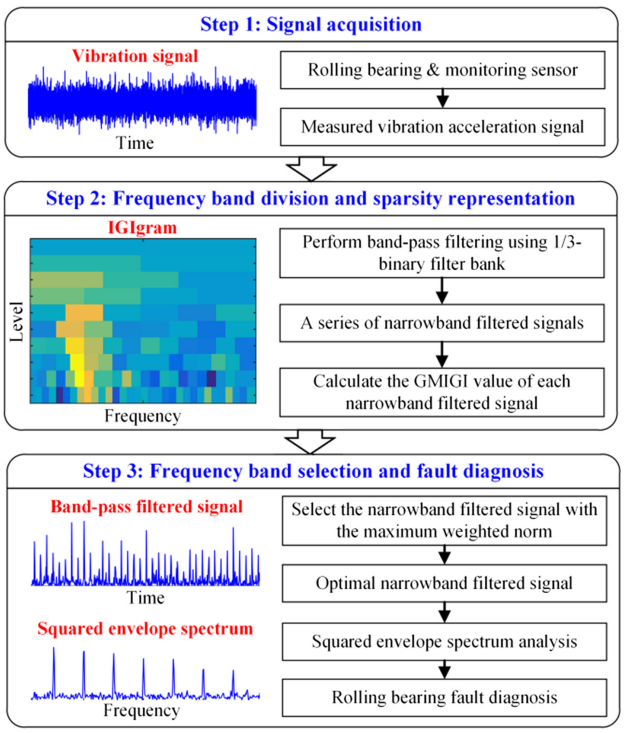


**Fig. 8.** Flowchart of proposed bearing fault diagnosis method.

*Step 3:* Calculate the squared envelope and SES of the narrowband filtered signal and calculate the GMIGI value of each narrowband filtered signal.

*Step 4:* Select the optimal narrowband filtered signal from the obtained candidates by the maximum GMIGI criterion.

*Step 5:* Perform SES analysis on the selected narrowband filtered signal and identify bearing faults based on characteristic fault frequencies.

# IV. SIMULATION VERIFICATION

## A. NUMERICAL MODEL OF BEARING FAULT SIGNAL

A numerical simulation signal of bearing inner race fault is generated to validate the effectiveness of the IGIgram method in extracting repetitive transient features. The simulation signal considers the repetitive transient impulses caused by bearing defect shown in Eq. (13) and interference noises often encountered in industrial scenarios, including random transients in Eq. (14), discrete harmonics in Eq. (15) and background noise, as follows:

$$x(t) = x_1(t) + x_2(t) + x_3(t) + n(t) \tag{12}$$

$$x_1(t) = \sum_{i=1}^{97} e^{-1000(t-i/97-\Delta_i)} \sin(2\pi \cdot 5000(t-i/97-\Delta_i)) \tag{13}$$

$$x_2(t) = \sum_{j=1}^{3} A_j e^{-800(t-\tau_j)} \sin(2\pi \cdot 1700(t-\tau_j)) \tag{14}$$

$$x_3(t) = 0.1[\sin(2\pi \cdot 10t + \pi/6) + \sin(2\pi \cdot 20t - \pi/3)] \tag{15}$$

$$\Delta_i = \sum_{k=1}^{i} \delta_k, \qquad \delta_k \sim U(-\sqrt{3}/9700, \sqrt{3}/9700) \tag{16}$$

$$A_j = 2a_j, \qquad a_j \sim N(1,0.1) \tag{17}$$

$$\tau_j \sim U(0,1) \tag{18}$$

where $\Delta_i$ is the time jitter caused by the slippage effect of the rolling element [10,51]; $A_j$ and $\tau_j$ denote the amplitude and occurrence time of the $j$th random transient, respectively; $N(\cdot\,,\cdot)$ and $U(\cdot\,,\cdot)$ represent a normal distribution and a uniform distribution, respectively. In addition, the Gaussian noise with an SNR of −12.5 dB is added to simulate the background noise. The fault characteristic frequency of the bearing inner race is assumed to be 97 Hz. The sampling frequency and length are set to 12,800 Hz and 1 s, respectively.

## B. SIMULATION RESULTS

The simulation signal of bearing inner race fault and its magnitude spectrum and SES are depicted in Fig. 9. Only two discrete harmonics, 10 Hz and 20 Hz, can be detected in the magnitude spectrum, and the inner race fault characteristic frequency $f_i = 97$ Hz and its harmonics cannot be observed in SES.

To extract the repetitive transients, IGIs with power exponents $p = 0.1$, 0.3, 0.5, 0.8, 2, 3, 4 and 6 are introduced into the IGIgram method to select IFB. For comparison, Kurt, L2/L1, HI, GI and GGIs with $a = 0.1$, 0.3, 0.5, 0.8, 2, 3, 4 and 6 are employed to replace NE in the geometric infogram for selecting IFB. The decomposition level of the entire frequency band is set to 4 for all methods. Table I shows the frequency bands selected by different criteria on the simulation signal of bearing inner race fault. It can be observed that four different frequency bands are selected by these indicators. As some examples, Fig. 10 displays the geometric kurtogram, geometric infogram, IGIgram with $p = 0.8$ and IGIgram with $p = 3$. Furthermore, the envelopes and SESs of the band-pass filtered signal obtained from these four frequency bands are presented in Figs. 11 and 12, respectively.

Two large random impulses are exhibited in Fig. 11a, showing that Kurt and L2/L1 select the resonance frequency band of random impulses and fail to identify the resonance frequency band of repetitive transients.

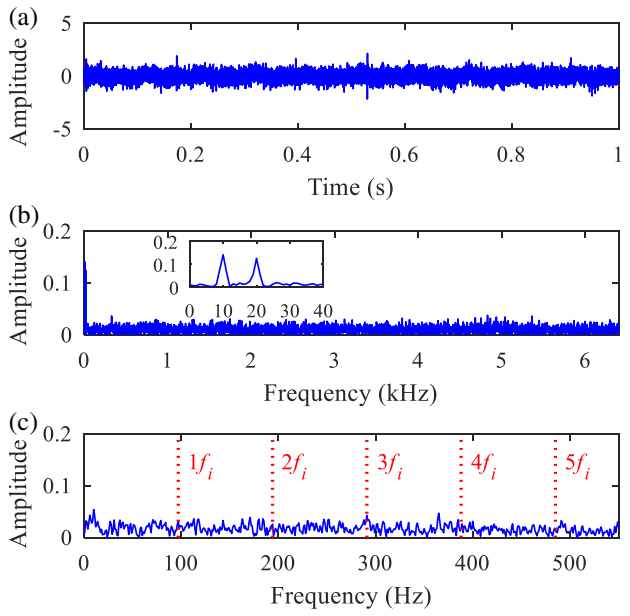


**Fig. 9.** Simulation of bearing inner race fault signal: (a) waveform, (b) magnitude spectrum and (b) SES.

**Table I.** Frequency bands selected by different criteria on the simulation signal of bearing inner race fault

| Criterion | Frequency band |
|---|---|
| Kurt, L2/L1 | (1800, 400) |
| NE, HI, GI, GGIs with $a = 0.1$, 0.3, 0.5 and 0.8, IGI with $p = 2$ | **(5,000, 400)** |
| GGIs with $a = 2$, 3, 4, 6, IGIs with $p = 0.1$, 0.3, 0.5 and 0.8 | (3,200, 6,400) |
| IGIs with $p = 3$, 4 and 6 | **(5,067, 533)** |

*Note:* (Central frequency, Bandwidth) in Hz.

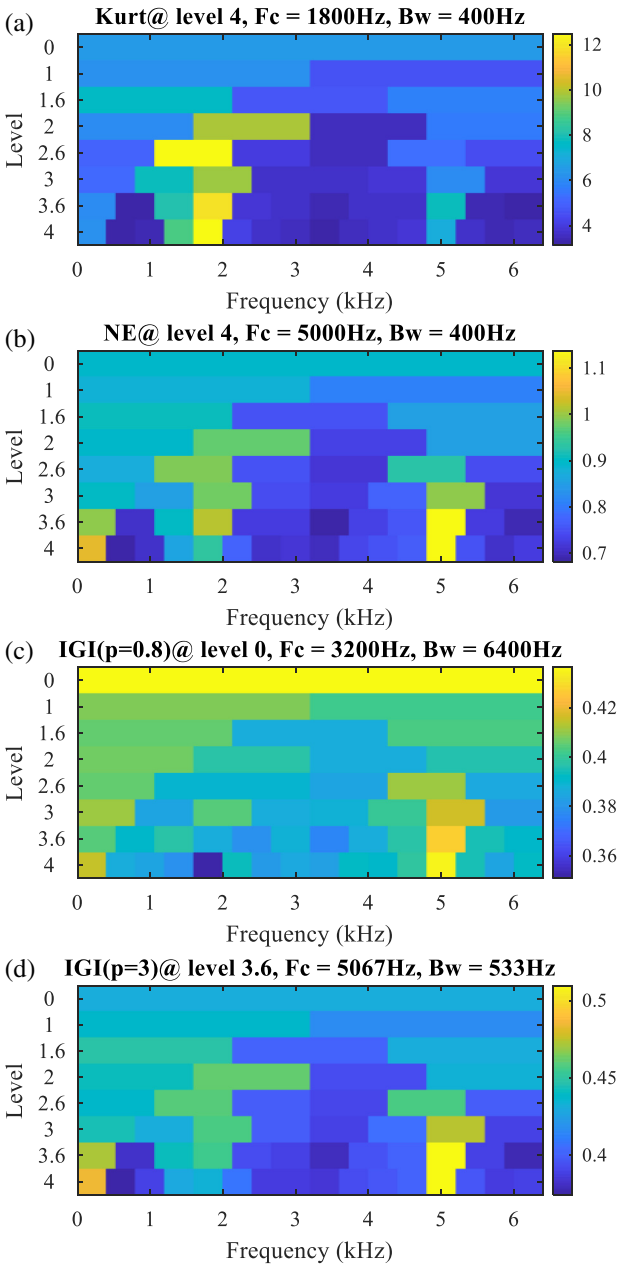


**Fig. 10.** (a) Geometric kurtogram, (b) geometric infogram, (c) IGIgram with $p = 0.8$ and (d) IGIgram with $p = 3$.

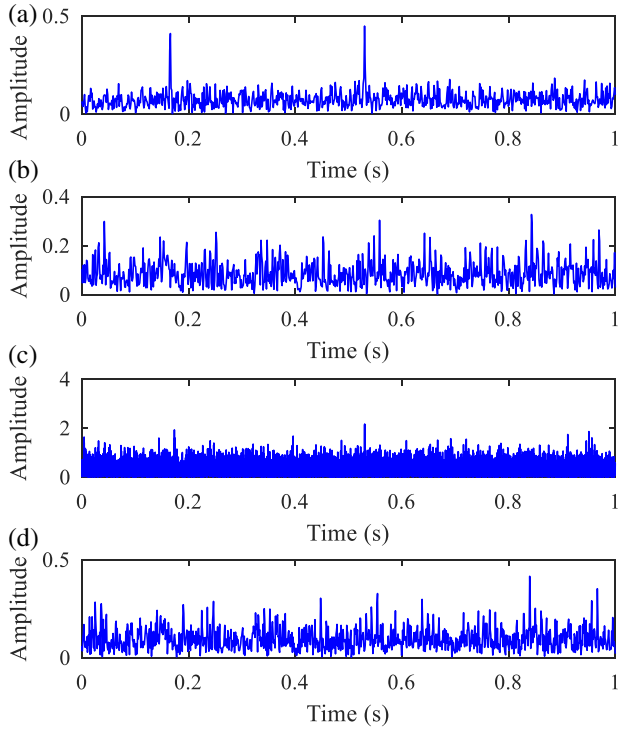


**Fig. 11.** Envelopes of the band-pass filtered signals obtained from different frequency bands: (a) band (1800, 400), (b) band (5,000, 400), (c) band (3200 6400) and (d) band (5,067, 533).

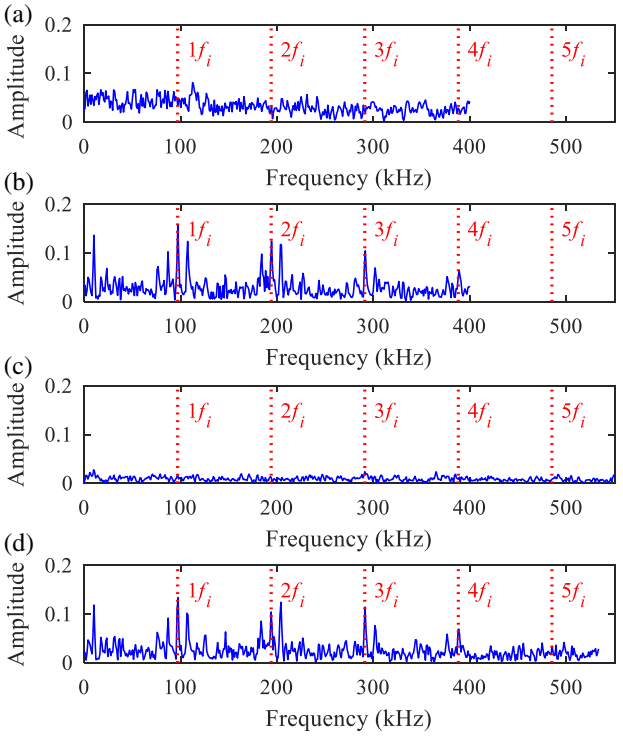


**Fig. 12.** SESs of the band-pass filtered signals obtained from different frequency bands: (a) band (1800, 400), (b) band (5,000, 400), (c) band (3200 6400) and (d) band (5,067, 533).

In contrast, the repetitive transient features can be observed in Fig. 11b, d and the inner race fault characteristic frequency $f_i = 97$ Hz and its harmonics can be easily detected in Fig. 12b, d. These results indicate that NE, HI, GI, GGIs with $a = 0.1$, 0.3, 0.5 and 0.8 and IGIs with $p = 2$, 3, 4 and 6 discriminate the correct resonance frequency bands (5,000, 400) and (5,067, 533). In addition, due to the wider frequency band, IGIs with $p = 3$, 4 and 6 achieve relatively good feature extraction results. The above results preliminarily verify the effectiveness of IGIs in identifying IFBs and extracting repetitive transient features.

## V. EXPERIMENTAL RESULTS

In this section, the vibration signals acquired from railway axle-box bearings under different operating conditions are used to validate the efficiency of the proposed fault diagnosis method, and the performance is compared with the improved geometric infogram based on state-of-the-art sparsity measures.

The experimental signals were collected from a railway axle-box bearing test rig. The test rig mainly consists of the driving device, wheelset mounted with axle-box bearings and loading device, as shown in Fig. 13a. The outer race fault and rolling element fault bearings were tested under different operating conditions. All bearing faults were implanted artificially with a depth of 0.2 mm and a width of 0.6 mm, as exhibited in Fig. 13b, c. The pitch diameter, rolling element diameter, number of rolling elements and contact angle of the tested axle-box bearings were 187.2 mm, 26.7 mm, 17 and 12.08°, respectively. Accelerometers were mounted along the vertical direction of the axle box to collect the vibration signals. The sampling

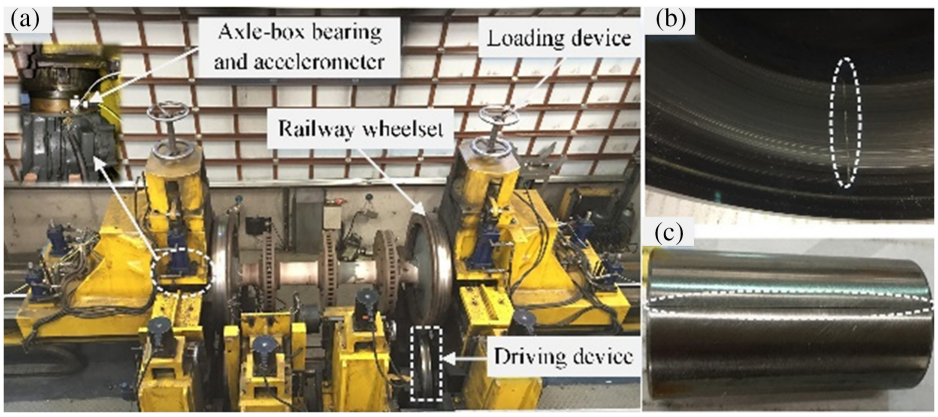


**Fig. 13.** (a) Railway axle-box bearing test rig, (b) damaged bearing outer race, and (c) damaged bearing rolling element.

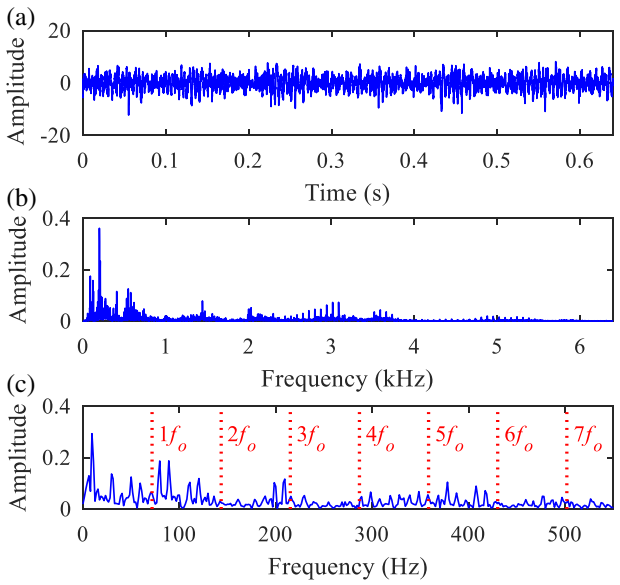


**Fig. 14.** Vibration signal of outer race fault bearing: (a) waveform, (b) magnitude spectrum and (c) SES.

**Table II.** Frequency bands selected by different criteria on the vibration signal of outer race fault bearing

| Criterion | Frequency band |
|---|---|
| Kurt | **(4,800, 3,200)** |
| NE, GI, GGIs with $a = 2$, 3, 4 and 6, IGIs with $p = 2$ and 3 | **(5,600, 1,600)** |
| L2/L1, HI, GGI with $a = 0.1$ | **(4,800, 1,067)** |
| GI, GGIs with $a = 0.3$, 0.5 and 0.8, IGIs with $p = 0.3$, 0.5 and 0.8 | **(5,067, 533)** |
| IGIs with $p = 0.1$ and 6 | (3,200, 6,400) |
| IGI with $p = 4$ | **(5,333, 2,133)** |

frequency and length of the vibration signal were set to 12.8 kHz and 8,192 sampling points, respectively.

## A. BEARING OUTER RACE FAULT

In this case, the vibration acceleration signal of the railway axle-box bearing with outer race fault is analyzed. The vibration signal was collected at a constant speed of 590 rpm, as shown in Fig. 14a. The transient impulse features induced by the bearing outer race fault are completely buried in the strong background noise, making it difficult to detect the fault characteristic frequency of the bearing outer race ($f_o = 71.88$ Hz) and its harmonics from SES shown in Fig. 14c.

The IGIgram using IGIs with $p = 0.1$, 0.3, 0.5, 0.8, 2, 3, 4 and 6 are employed to extract the fault impulse features of bearing outer race. The geometric infogram and its improved methods using Kurt, L2/L1, HI, GI and GGIs with $a = 0.1$, 0.3, 0.5, 0.8, 2, 3, 4 and 6 are also applied to the signal in Fig. 14a for comparison. The decomposition level of the entire frequency band is set to 4 for all methods. Table II shows the six frequency bands selected by different criteria for bearing outer race fault diagnosis. The envelopes and SESs of the band-pass filtered signals obtained from six selected frequency bands are displayed in Figs. 15 and 16, respectively.

The repetitive impulse features can be clearly observed in Fig. 15a–f, and the outer race fault characteristic frequency $f_o$ and its first six harmonics can be easily detected in Fig. 16a–d and f. These results indicate that five frequency bands (4,800, 3,200), (5,600, 1,600), (4,800, 1,067), (5,067, 533) and (5,333, 2,133) contain repetitive impulse features caused by bearing outer race fault. Because the frequency bands (5,600, 1,600), (4,800, 1,067) and (5,067, 533) have relatively narrow bandwidths, the SESs of their corresponding filtered signals exhibit better fault diagnosis effects. In addition, IGIs with $p = 0.1$ and 6 fail to effectively identify the fault-related resonance frequency bands, which may be caused by the weaker repetitive transient discriminability of IGI with $p = 0.1$ and the susceptibility to the noise of IGI with $p = 6$. These results verify the effectiveness of IGIs in fault diagnosis of axle-box bearing outer race and also show that the power exponent of IGIs should not be too large or too small in the application.

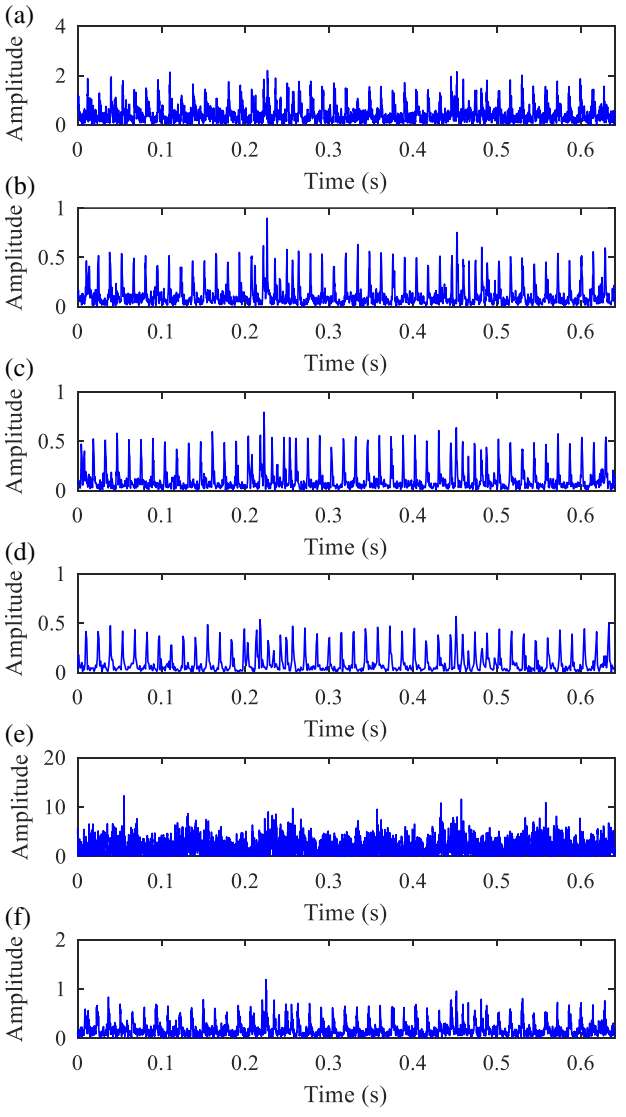


**Fig. 15.** Envelopes of the band-pass filtered signals obtained from different frequency bands: (a) band (4,800, 3,200), (b) band (5,600, 1,600), (c) band (4,800, 1,067), (d) band (5,067, 533), (e) band (3,200, 6,400) and (g) band (5,333, 2,133).

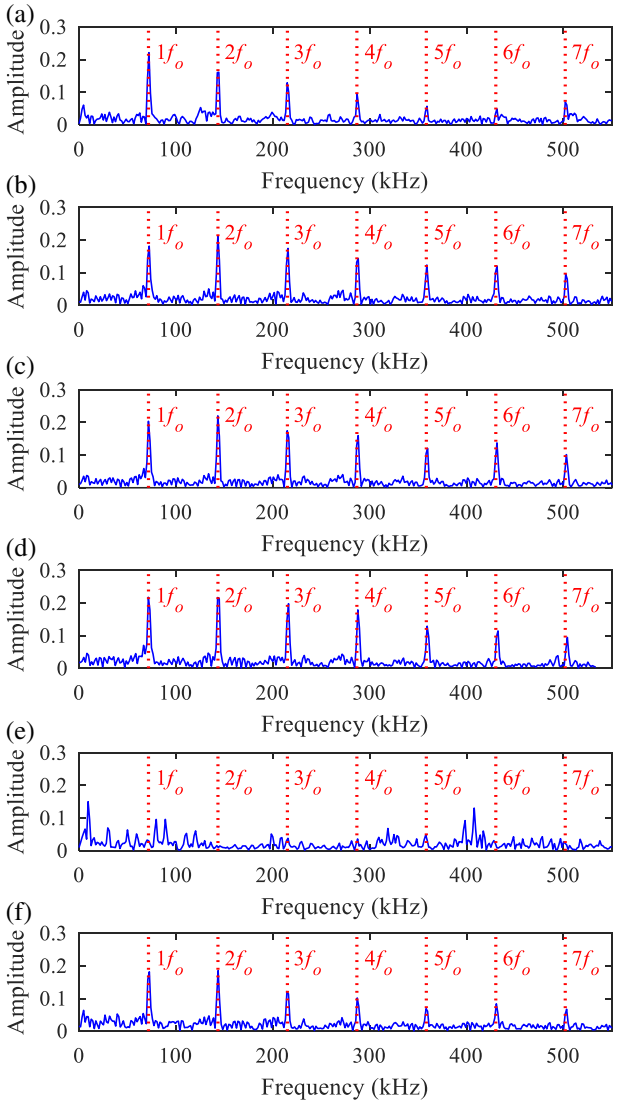


**Fig. 16.** SESs of the band-pass filtered signals obtained from different frequency bands: (a) band (4,800, 3,200), (b) band (5,600, 1,600), (c) band (4,800, 1,067), (d) band (5,067, 533), (e) band (3,200, 6,400) and (g) band (5,333, 2,133).

## B. BEARING ROLLING ELEMENT FAULT

The vibration signal of the rolling element fault bearing collected at a constant speed of 885 rpm is used to further validate the proposed method, as displayed in Fig. 17a. The repetitive impulse features induced by the rolling element fault are buried in the strong background noise. Although the harmonics $2f_b$, $3f_b$ and $6f_b$ can be observed from SES shown in Fig. 17c, the fault characteristic frequency of the bearing rolling element ($f_b = 48.15$ Hz) and other harmonics are not obvious, resulting in the inability to accurately judge the health status of the axle-box bearing.

To extract the fault impulse features of bearing rolling element, the IGIgram using IGIs with $p = 0.1$, 0.3, 0.5, 0.8, 2, 3, 4 and 6, geometric infogram and its improved methods using Kurt, L2/L1, HI, GI and GGIs with $a = 0.1$, 0.3, 0.5, 0.8, 2, 3, 4 and 6 are applied to the vibration signal shown in Fig. 17a. The decomposition level of the entire frequency band is set to 4 for all methods. Table III displays the six frequency bands selected by different criteria for fault diagnosis of bearing rolling element. Figs. 18 and 19

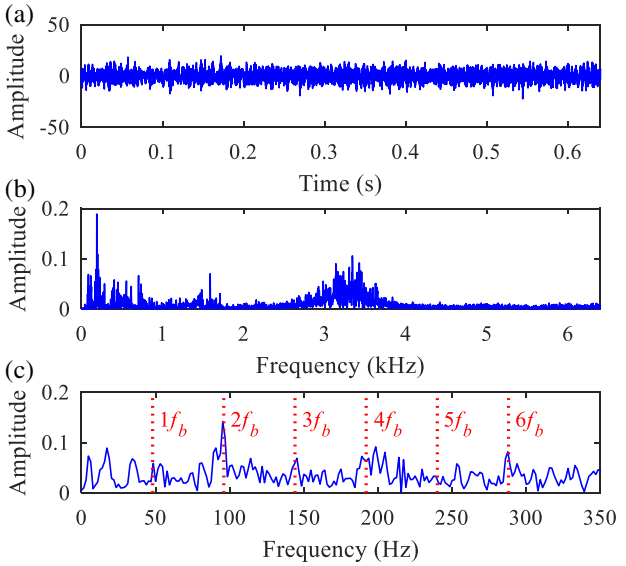


**Fig. 17.** Vibration signal of rolling element fault bearing: (a) waveform, (b) magnitude spectrum and (c) SES.

**Table III.** Frequency bands selected by different criteria on the vibration signal of rolling element fault bearing

| Criterion | Frequency band |
|---|---|
| Kurt | **(5,867, 1,067)** |
| NE | **(5,200, 800)** |
| L2/L1, HI, GGIs with $a = 0.1$, 0.3, 0.5 and 0.8, IGI with $p = 2$ | **(5,400, 400)** |
| GI, GGIs with $a = 2$, 3, 4 and 6, IGI with $p = 0.8$ | (4,000, 1,600) |
| IGIs with $p = 0.1$, 0.3 and 0.5 | (3,200, 6,400) |
| IGIs with $p = 3$, 4 and 6 | **(5,600, 1,600)** |

show the envelopes and SESs of the band-pass filtered signals obtained from the six selected frequency bands, respectively.

As shown in Fig. 18a–c and f, the repetitive impulse features can be clearly observed. Correspondingly, in Fig. 19a–c and f, the fault characteristic frequency of bearing rolling element $f_b$ and its first three harmonics can be easily identified, and the sidebands can also be detected. Thus, the results obtained from the band frequency bands (5,867, 1,067), (5,200, 800), (5,400, 400) and (5,600, 1,600) confirm the rolling element fault of the axle-box bearing. Furthermore, the SESs obtained from the frequency bands (5,867, 1,067) and (5,600, 1,600) achieve better effects than that of the other two frequency bands. The above results further verify the effectiveness of IGIs in IFB identification and bearing fault diagnosis.

# VI. COMPARISON WITH LOG-CYCLIGRAM

To further illustrate the performance of the proposed method in bearing fault diagnosis, a state-of-the-art

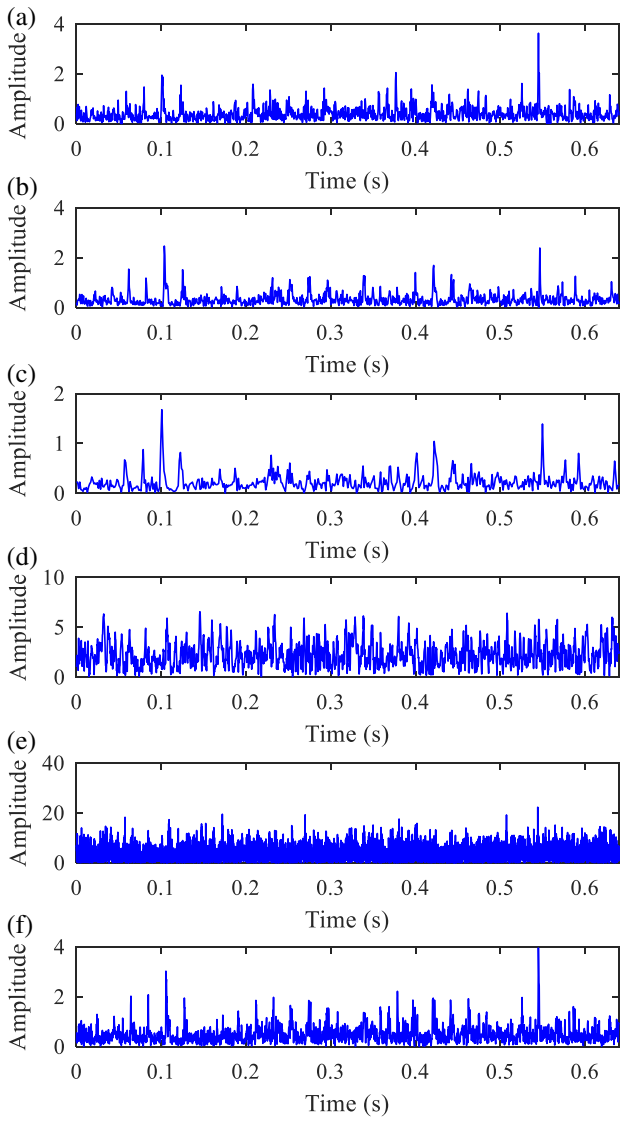


**Fig. 18.** Envelopes of the band-pass filtered signals obtained from different frequency bands: (a) band (5,867, 1,067), (b) band (5,200, 800), (c) band (5,400, 400), (d) band (4,000, 1,600) (e) band (3,200, 6,400) and (f) band (5,600, 1,600).

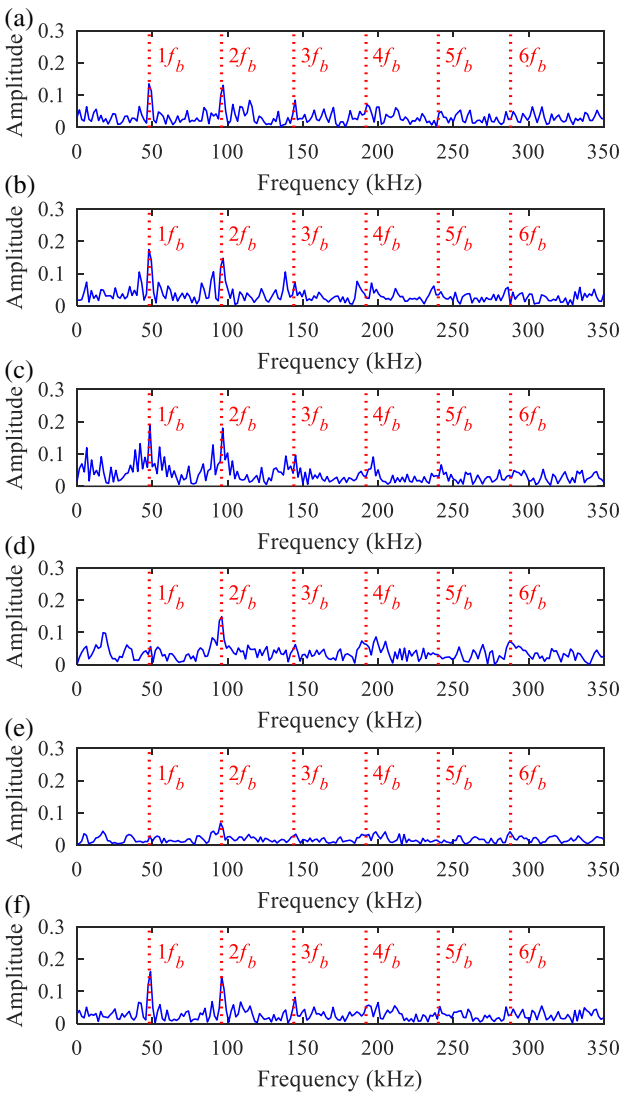


**Fig. 19.** SES of the band-pass filtered signals obtained from different frequency bands: (a) band (5,867, 1,067), (b) band (5,200, 800), (c) band (5,400, 400), (d) band (4,000, 1,600) (e) band (3,200, 6,400) and (f) band (5,600, 1,600).

envelope analysis method, LC [12], is applied to the simulation and experimental signals in Sections IV and V for comparison. The decomposition level of the entire frequency band is also set to 4. The bearing fault characteristic frequency calculated from the nominal speed and bearing geometric parameters is used as an input parameter of the LC method to guide the frequency band selection. Fig. 20 shows the frequency bands selected by the LC method on the simulation signal in Fig. 9a and experimental signals in Figs. 14a, and 17a, which are (5,000, 400), (4,600, 400) and (5,000, 400) respectively. Figs. 21 and 22 display the envelopes and SESs of the band-pass filtered signals for processing the simulation signal of bearing inner race fault, the experimental signal of bearing outer race fault and the experimental signal of bearing rolling element fault, respectively.

As shown in Fig. 21, the repetitive transient features can be observed in the envelopes of the band-pass filtered signals. In Fig. 22, the bearing fault characteristic frequencies and their harmonics (indicated by the red dotted lines) can be detected in the SESs of the band-pass filtered signals. These results show that the LC method effectively extracts the transient features related to different bearing faults. Nevertheless, only the rolling element fault characteristic frequency $1f_b$ and its harmonic $2f_b$ can be clearly observed in Fig. 22c and the other harmonics are not prominent, which seems to be slightly inferior to the results shown in Fig. 19c, and f, where $3f_b$ and even other harmonics can be detected. In addition, it should be pointed out that IGIgram can adaptively extract fault-related transient features, unlike the LC method which aims to extract repetitive transient features with a specified characteristic frequency. This shows that the IGIgram with appropriate power exponent $p$ can achieve a fault diagnosis effect similar to the LC method and has advantages in the adaptive extraction of bearing fault features.

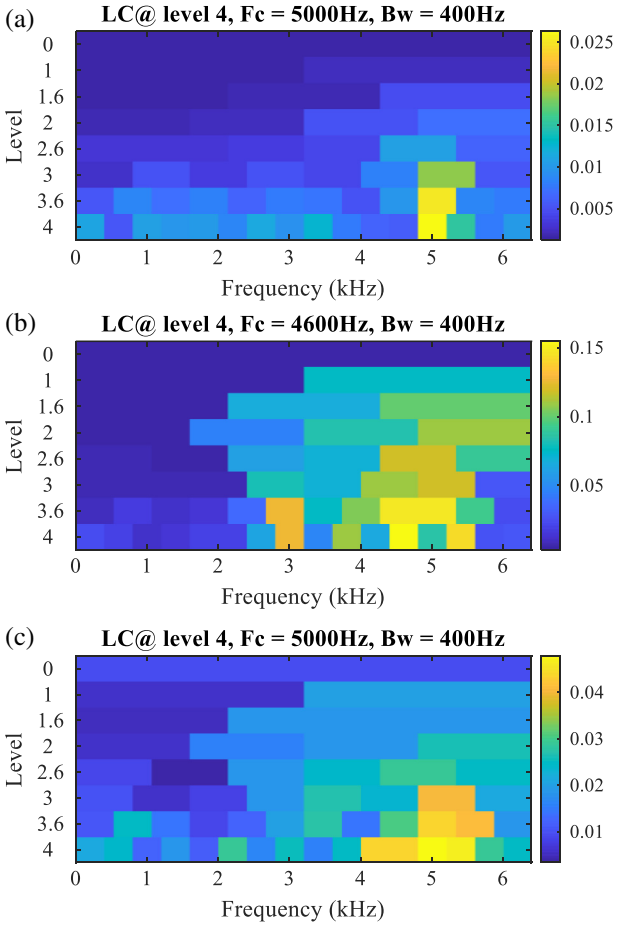


**Fig. 20.** Log-cycligrams of different signals: (a) simulation signal of bearing inner race fault, (b) experimental signal of bearing outer race fault and (c) experimental signal of bearing rolling element fault.

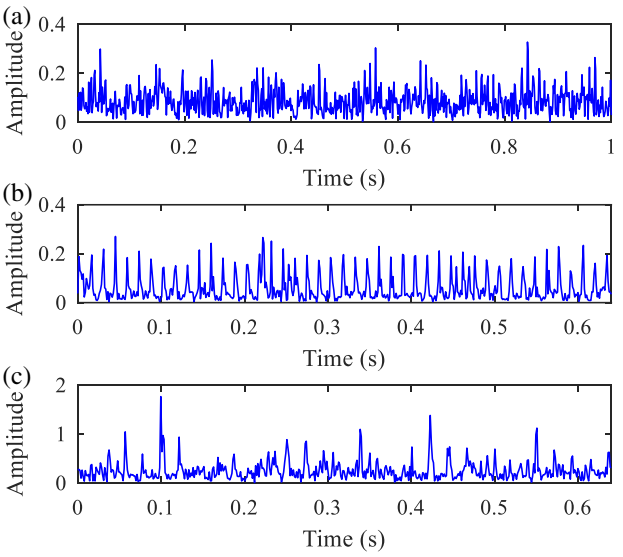


**Fig. 21.** Envelopes of the band-pass filtered signals obtained by LC on different signals: (a) simulation signal of bearing inner race fault, (b) experimental signal of bearing outer race fault and (c) experimental signal of bearing rolling element fault.

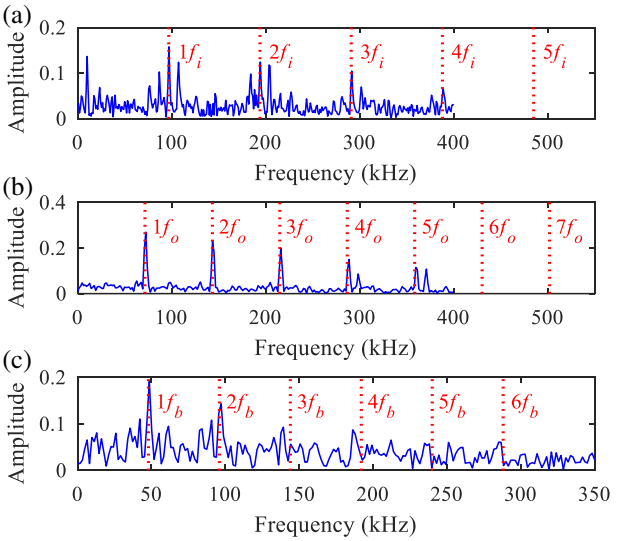


**Fig. 22.** SES of the band-pass filtered signals obtained by LC on different signals: (a) simulation signal of bearing inner race fault, (b) experimental signal of bearing outer race fault and (c) experimental signal of bearing rolling element fault.

## VII. CONCLUSIONS

In this paper, a generalization method of the classic GI is developed from the perspective of the quasi-arithmetic mean generator, and IGIs are proposed as new statistical indicators for sparse quantification. Further, the IFBI method that uses IGI as the fault information metric, named IGIgram, is introduced for envelope analysis-based bearing fault diagnosis. Simulations and experiments are conducted to verify the performance of IGIs and IGIgram against the typical sparsity measures. The following important conclusions can be drawn:

(1) The proposed generalization method of classic GI is reasonable and effective. IGIs can monotonically quantify the sparsity of the signal and can achieve strong repetitive transient discriminability under noise contamination.

(2) The IGIgram method using IGI with appropriate power exponent can accurately discriminate IFB of the vibration signals to extract repetitive transients for bearing fault diagnosis.

(3) Compared with Kurt, L2/L1 and GI, IGIs with power exponents $p = 2$, 3 and 4 exhibit high random transient resistibility and strong repetitive transient discriminability simultaneously, therefore they are recommended for applications.

In future work, the performance comparison of IGIgram and other targeted IFBI methods in rotating machinery fault diagnosis is worth investigating. The fault diagnosis performance of IGIgram based on the log-envelope spectrum is also worth exploring. Furthermore, IGIs can be used to develop machine fault feature extraction methods and condition monitoring methods.

## ACKNOWLEDGMENTS

This work was supported by the National Key Research and Development Program of China (Grant No. 2019YFB1405401),

the National Natural Science Foundation of China (Grant No. P110520G02004) and the China Scholarship Council (Grant No. 202107000033), which are highly appreciated by the authors.

## CONFLICT OF INTEREST STATEMENT

The authors declare no conflicts of interest.

## References


1. A. Rai and S. H. Upadhyay, "A review on signal processing techniques utilized in the fault diagnosis of rolling element bearings," *Tribol. Int.*, vol. 96, pp. 289–306, 2016.
2. Y. Miao, B. Zhang, J. Lin, M. Zhao, and H. Liu, "A review on the application of blind deconvolution in machinery fault diagnosis," *Mech. Syst. Signal Process.*, vol. 163, p. 108202, 2022.
3. W. Zhou, Z. Feng, Y. F. Xu, X. Wang, and H. Lv, "Empirical fourier decomposition: an accurate signal decomposition method for nonlinear and non-stationary time series analysis," *Mech. Syst. Signal Process.*, vol. 163, p. 118155, 2022.
4. J. Antoni, "Fast computation of the kurtogram for the detection of transient faults," *Mech. Syst. Signal Process.*, vol. 21, pp. 108–124, 2007.
5. Z. Qiao, Y. Lei, and N. Li, "Applications of stochastic resonance to machinery fault detection: a review and tutorial," *Mech. Syst. Signal Process.*, vol. 122, pp. 502–536, 2019.
6. W. Zhang, P. Shi, M. Li, and D. Han, "A novel stochastic resonance model based on bistable stochastic pooling network and its application," *Chaos Solitons Fractals*, vol. 145, p. 110800, 2021.
7. B. Chen, Y. Cheng, W. Zhang, and G. Mei, "Investigation on enhanced mathematical morphological operators for bearing fault feature extraction," *ISA Trans.*, 2021, in press. doi: https://doi.org/10.1016/j.isatra.2021.07.027.
8. J. Antoni, G. Xin, and N. Hamzaoui, "Fast computation of the spectral correlation," *Mech. Syst. Signal Process.*, vol. 92, pp. 248–277, 2017.
9. B. Chen, Y. Cheng, W. Zhang, and F. Gu, "Enhanced bearing fault diagnosis using integral envelope spectrum from spectral coherence normalized with feature energy," *Measurement*, vol. 189, p. 110448, 2021.
10. X. Tian, J. Xi Gu, I. Rehab, G. M. Abdalla, F. Gu, and A. D. Ball, "A robust detector for rolling element bearing condition monitoring based on the modulation signal bispectrum and its performance evaluation against the Kurtogram," *Mech. Syst. Signal Process.*, vol. 100, pp. 167–187, 2018.
11. P. D. McFadden and J. D. Smith, "Vibration monitoring of rolling element bearings by the high-frequency resonance technique – a review," *Tribol. Int.*, vol. 17, pp. 3–10, 1984.
12. W. A. Smith, P. Borghesani, Q. Ni, K. Wang, and Z. Peng, "Optimal demodulation-band selection for envelope-based diagnostics: a comparative study of traditional and novel tools," *Mech. Syst. Signal Process.*, vol. 134, p. 106303, 2019.
13. T. Barszcz and A. Jabło□ski, "A novel method for the optimal band selection for vibration signal demodulation and comparison with the Kurtogram," *Mech. Syst. Signal Process.*, vol. 25, pp. 431–451, 2011.
14. A. Moshrefzadeh and A. Fasana, "The Autogram: an effective approach for selecting the optimal demodulation band in rolling element bearings diagnosis," *Mech. Syst. Signal Process.*, vol. 105, pp. 294–318, 2018.
15. K. Zhang, Y. Xu, Z. Liao, L. Song, and P. Chen, "A novel Fast Entrogram and its applications in rolling bearing fault diagnosis," *Mech. Syst. Signal Process.*, vol. 154, p. 107852, 2021.
16. P. Tse and D. Wang, "The design of a new sparsogram for fast bearing fault diagnosis: Part 1 of the two related manuscripts that have a joint title as 'two automatic vibration-based fault diagnostic methods using the novel sparsity measurement - Parts 1 and 2'," *Mech. Syst. Signal. Process.*, vol. 40, pp. 499–519, 2013.
17. P. Hoyer, "Non-negative matrix factorization with sparseness constraints," *J. Mach. Learn. Res.*, vol. 5, pp. 1457–1469, 2004.
18. J. Antoni, "The infogram: entropic evidence of the signature of repetitive transients," *Mech. Syst. Sig. Process.*, vol. 74, pp. 73–94, 2016.
19. J. Hebda-Sobkowicz, R. Zimroz, A. Wyłoma□ska, and J. Antoni, "Infogram performance analysis and its enhancement for bearings diagnostics in presence of non-Gaussian noise," *Mech. Syst. Signal Process.*, vol. 170, p. 108764, 2022.
20. Y. Miao, M. Zhao, and J. Lin, "Improvement of kurtosis-guided-grams via Gini index for bearing fault feature identification," *Meas. Sci. Technol.*, vol. 28, p. 125001, 2017.
21. D. Wang, "Some further thoughts about spectral kurtosis, spectral L2/L1 norm, spectral smoothness index and spectral Gini index for characterizing repetitive transients," *Mech. Syst. Signal Process.*, vol. 108, pp. 58–72, 2018.
22. Y. Miao, M. Zhao, and J. Hua, "Research on sparsity indexes for fault diagnosis of rotating machinery," *Measurement*, vol. 158, p. 107733, 2020.
23. S. Liu, S. Hou, K. He, and W. Yang, "L-Kurtosis and its application for fault detection of rolling element bearings," *Measurement*, vol. 116, pp. 523–532, 2018.
24. G. □ak, A. Wyłoma□ska, and R. Zimroz, "Application of alpha-stable distribution approach for local damage detection in rotating machines," *J. Vibroeng.*, vol. 17, pp. 2987–3002, 2015.
25. J. Hebda-Sobkowicz, R. Zimroz, M. Pitera, and A. Wyłoma□ska, "Informative frequency band selection in the presence of non-Gaussian noise – a novel approach based on the conditional variance statistic with application to bearing fault diagnosis," *Mech. Syst. Signal Process.*, vol. 145, p. 106971, 2020.
26. K. Liang, M. Zhao, J. Lin, C. Ding, J. Jiao, and Z. Zhang, "A novel indicator to improve fast kurtogram for the health monitoring of rolling bearing," *IEEE Sens. J.*, vol. 20, pp. 12252–12261, 2020.
27. L. Wang, Z. Liu, H. Cao, and X. Zhang, "Subband averaging kurtogram with dual-tree complex wavelet packet transform for rotating machinery fault diagnosis," *Mech. Syst. Signal Process.*, vol. 142, p. 106755, 2020.
28. J. Hebda-Sobkowicz, R. Zimroz, and A. Wyłomanska, "Selection of the informative frequency band in a bearing fault diagnosis in the presence of non-gaussian noise-Comparison of recently developed methods," *Appl. Sci.*, vol. 10, p. 2657, 2020.
29. A. P. Daga, L. Garibaldi, A. Fasana, and S. Marchesiello, "Performance of envelope demodulation for bearing damage detection on cwru accelerometric data: Kurtogram and traditional indicators vs. targeted a posteriori band indicators," *Appl. Sci.*, vol. 11, p. 6262, 2021.
30. X. Xu, M. Zhao, J. Lin, and Y. Lei, "Envelope harmonic-to-noise ratio for periodic impulses detection and its application to bearing diagnosis," *Measurement*, vol. 91, pp. 385–397, 2016.

31. X. Zhang, J. Kang, L. Xiao, J. Zhao, and H. Teng, "A new improved kurtogram and its application to bearing fault diagnosis," *Shock Vib.*, 2015, pp. 1–22, 2015.
32. Z. Liu, S. Yang, Y. Liu, J. Lin, and X. Gu, "Adaptive correlated Kurtogram and its applications in wheelset-bearing system fault diagnosis," *Mech. Syst. Signal Process.*, vol. 154, p. 107511, 2021.
33. P. Borghesani, P. Pennacchi, and S. Chatterton, "The relationship between kurtosis- and envelope-based indexes for the diagnostic of rolling element bearings," *Mech. Syst. Signal Process.*, vol. 43, pp. 25–43, 2014.
34. W. A. Smith, R. B. Randall, S. du Mée X de, and P. Peng, "Use of cyclostationary properties to diagnose planet bearing faults in variable speed conditions," Presented at 10th DST Group Int. Conf. Health Usage Monit. Syst., Melbourne, Australia, 26 February 2017 – 28 February 2017. Available: http://www.humsconference.com.au/Papers2017/Peer_Reviewed/210_HUM2017_Randall.pdf.
35. X. Gu, S. Yang, Y. Liu, and R. Hao, "Rolling element bearing faults diagnosis based on kurtogram and frequency domain correlated kurtosis," *Meas. Sci. Technol.*, vol. 27, p. 125019, 2016.
36. Z. Mo, J. Wang, H. Zhang, and Q. Miao, "Weighted cyclic harmonic-to-noise ratio for rolling element bearing fault diagnosis," *IEEE Trans. Instrum. Meas.*, vol. 69, pp. 432–442, 2020.
37. P. Borghesani and M. R. Shahriar, "Cyclostationary analysis with logarithmic variance stabilization," *Mech. Syst. Signal Process.*, vol. 70–71, pp. 51–72, 2016.
38. J. Antoni and P. Borghesani, "A statistical methodology for the design of condition indicators," *Mech. Syst. Signal Process.*, vol. 114, pp. 290–327, 2019.
39. C. Luo, Z. Mo, and Q. Miao, "Cyclic harmonic ratio defined in squared envelope spectrum and log-envelope spectrum for gearbox fault diagnosis," *IEEE Trans. Instrum. Meas.*, vol. 69, pp. 9568–9577, 2020.
40. X. He, Q. Liu, W. Yu, C. K. Mechefske, and X. Zhou, "A new autocorrelation-based strategy for multiple fault feature extraction from gearbox vibration signals," *Measurement*, vol. 171, p. 108738, 2021.
41. Q. Ni, J. C. Ji, K. Feng, and B. Halkon, "A novel correntropy-based band selection method for the fault diagnosis of bearings under fault-irrelevant impulsive and cyclostationary interferences," *Mech. Syst. Sig. Process.*, vol. 153, p. 107498, 2021.
42. H. Alavi, A. Ohadi, and S. T. Niaki, "A novel targeted method of informative frequency band selection based on lagged information for diagnosis of gearbox single and compound faults," *Mech. Syst. Signal Process.*, vol. 170, p. 108828, 2022.
43. D. Wang, Z. Peng, and L. Xi, "The sum of weighted normalized square envelope: a unified framework for kurtosis, negative entropy, Gini index and smoothness index for machine health monitoring," *Mech. Syst. Signal Process.*, vol. 140, p. 106725, 2020.
44. B. Hou, D. Wang, T. Xia, Y. Wang, Y. Zhao, and K. L. Tsui, "Investigations on quasi-arithmetic means for machine condition monitoring," *Mech. Syst. Signal Process.*, vol. 151, p. 107451, 2021.
45. B. Hou, D. Wang, T. Xia, L. Xi, Z. Peng, and K. L. Tsui, "Generalized Gini indices: complementary sparsity measures to Box-Cox sparsity measures for machine condition monitoring", *Mech. Syst. Signal Process.*, vol. 169, p. 108751, 2022.
46. B. Hou, D. Wang, T. Yan, Y. Wang, Z. Peng, and K. L. Tsui, "Gini indices II and III: Two new sparsity measures and their applications to machine condition monitoring," *IEEE/ASME Trans. Mechatron.*, 2021, in press. doi: https://doi.org/10.1109/TMECH.2021.3100532.
47. N. Hurley and S. Rickard, "Comparing measures of sparsity," *IEEE Trans. Inf. Theory*, vol. 55, pp. 4723–4741, 2009.
48. R. F. Dwyer, "Detection of non-Gaussian signals by frequency domain kurtosis estimation," *ICASSP, IEEE Int. Conf. Acoust. Speech Signal Process. Proceed.*, vol. 2, pp. 607–610, 1983.
49. C. Gini, "Measurement of inequality of incomes," *Econom. J.*, vol. 31, pp. 124–126, 1921.
50. B. Hou, D. Wang, T. Yan, and Z. Peng, "A comparison of machine health indicators based on the impulsiveness of vibration signals," *Acoust. Aust.*, vol. 49, pp. 199–206, 2021.
51. R. B. Randall and J. Antoni, "Rolling element bearing diagnostics-A tutorial," *Mech. Syst. Signal Process.*, vol. 25, pp. 485–520, 2011.